Journal of the Brazilian Society of Mechanical Sciences and Engineering (2020) 42:41
https://doi.org/10.1007/s40430-019-2117-9

TECHNICAL PAPER

Assessment of the performance of airflow in an operating rooms using ceiling supply and sidewall inlet systems

T. M. Baracat[1] · C. A. da Silva[1] · F. C. Lofrano[1] · F. A. Kurokawa[1]

Received: 14 August 2019 / Accepted: 1 December 2019 / Published online: 12 December 2019

Abstract
Poor air quality arises by and large from inadequate ventilation and presence of contaminants. In particular to hospital environments, it exercises direct and significant influence over infections occurrence. The purpose of this paper is to research, through computational fluid dynamics, how ceiling (four-way supply) and sidewall (conventional high supply) inlets systems, as well as outlet (exhaust) positioning, effect air motion and distribution in operating rooms. By the assistance of numerical modeling, four alternative scenarios of a operating room were investigated, maintaining flow rates and varying inlet system and outlet position. The results are presented in terms of velocity vectors and temperatures, which were compared to the experimental data available. Subsequently, a qualitative analysis regarding conformity to sanitary requirements was conducted.

Keywords Computational fluid dynamics · Numerical simulation · Airflow · Indoor air quality · Operating rooms

1 Introduction

Adopted to provide thermal comfort and ventilation, air distribution system is intended to contribute for space occupant's well-being and processes' increased performance. Although associated with a subjective evaluation, user's satisfaction toward the enclosed environment is only achieved by HVAC (heating, ventilation and air conditioning) engineering. In this context, it is fundamental that air distribution devices—namely, inlets and outlets—are set to meet room requirements, depending upon the space use (e.g., residence, office, hospital, school, and hotel).

When it comes to hospital facilities, in addition to thermal comfort, sanitary quality also plays a major role, being of utmost importance in view of reducing or eradicating air contamination. Aerial contamination is considered to be one of the main causes of contract diseases by patients, health professionals and visitors [8, 30, 35, 38]. In this way, operating rooms appear as a sector of major relevance. According to Gosdena, Macgowana and Bannister [17], the number of people in the surgical environment and the air distribution system affects contamination level.

In particular to this matter, air outlets, such as exhausts (return air), are responsible for the elimination and treatment of the contaminated air of surgical rooms. Hence, the selection and the location of outlet devices should not be sidelined [18, 21, 25, 39]. In relation to its selection, American Society of Heating, Refrigerating and Air-conditioning Engineers—ASHRAE [3] indicates that it depends on (a) velocity in the occupied zone near outlets, (b) permissible pressure drop, and (c) noise.

In terms of velocity, it decreases as distance from extract increases, reason why drafty conditions are rare to occur near outlets. Also, it does not exert influence in airflow patterns beyond a distance of one characteristic length (e.g., square root of the inlet area) from outlet. Regarding pressure drop and noise, they should be in accordance with local standards [3].

Technical Editor: Daniel Onofre de Almeida Cruz, D.Sc.

✉ F. A. Kurokawa
fernando.kurokawa@usp.br

T. M. Baracat
thais.baracat@usp.br

C. A. da Silva
cibele.vas@usp.br

F. C. Lofrano
fabio.lofrano@usp.br

[1] Departamento de Engenharia de Construção Civil, Escola Politécnica, Universidade de São Paulo, São Paulo, Brazil

Concerning its location, ASHRAE [2] highlights that air outlets should be positioned to minimize short-circuiting of supply air. ASHRAE [3] points out that, in case air suppliers are attached to the ceiling, outlets should be positioned between the jets and at the side of the room, away from supply jets.

For inlet systems, ASHRAE [2] argues that different types of inlets are suitable for health care facilities. ASHRAE [3] points out that inlets mounted in or near the ceiling that discharge air horizontally (Group A inlets) are suited for cooling purposes, as desired in hospital environments. Figure 1 presents air motion from sidewall and ceiling inlet.

ASHRAE [3] presents sidewall inlets with discharge angle of 0° as having a longer throw and a greater drop compared to 360° angle ceiling diffuser. Similar inlets with other angles may have their performance between these two extremes. In addition, for an optimum diffusion in areas with normal ceilings, supply air should scrub the ceiling surface

The choice of inlets is essentially influenced by local sources of heat gain or loss, which promote convection currents or cause stratification. ASHRAE [2] indicates that square plaque diffusers are ideally used in less-critical areas to radial flow, whereas laminar diffusers for more-critical spaces. Low-velocity and laminar flow diffusers are believed to suit better operating rooms. However, adjustable-angle inlets may be preferable, once they allow field adjustments and adequacy to cool-air-sensitive patients.

In the literature, studies concerning airflow analysis are essentially subdivided into experimental (e.g., [9, 12, 24, 33, 34]) and mathematical models ([28, 29]). In this domain, researchers have been opting by and large for numerical modeling, given its reproducibility and realistic approach when it comes to the design of case studies. Besides, exclusive experimental studies have constructive and financial limitations, which narrow the range of scenarios to be assessed. Moreover, due to its mathematical limitation, the analytical approach presents some difficulty when it comes to the simultaneous analysis of multiple variables, such as those encountered in air inlets and outlets.

A particular numerical approach, which has been largely exploited to airflow analysis in indoor space, is the computational fluid dynamics (CFD). This approach has the advantage to promote alternatives to experimental researches. In addition, it can also complement studies in basic project phase, such as highlighted by Posner, Buchanan and Dunn-Rankin [30], who mentioned its resourcefulness to define operating rooms' layout. Indeed, the possibility to preview airflow and temperature distribution previously to the construction entails to a wise decision-making, optimizing the performance of the air system and improving thermal comfort and environment's safety.

In this context, our motivation in the present work is to investigate, through CFD simulation, the influence and the performance of ceiling (four-way supply) and sidewall (conventional high supply) inlets systems, as well as outlet (exhaust) positioning, with respect to air motion and distribution in operating rooms. The numerical modeling is validated, by comparing its results to the experimental data collected. Furthermore, by the assistance of numerical modeling, four alternative scenarios of a operating room were investigated, maintaining flow rates and varying inlet system and outlet position.

The paper is organized as follows. In Sect. 2, the modeling of operating room is described. The mathematical setting for airflow and boundary conditions adopted for solving these equations and computational approach are presented in Sect. 3. The next section gives description of the field measurements and geometric modeling. Numerical results

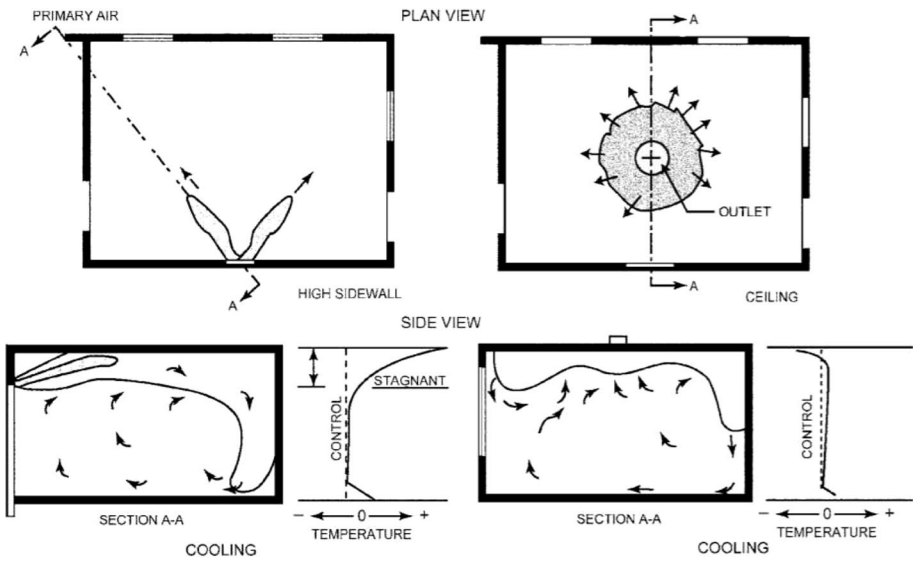

Fig. 1 Air motion characteristics from Group A inlets. *Source* [3]

are presented and discussed in Sect. 5. Finally, some concluding remarks are presented in the last section.

2 Modeling of operating room

The operating room considered in this work is located in the Hospital of the University of São Paulo. Its dimensions of 5.70 m × 5.40 m × 3.14 m (length × width × height), result in an area of 30.78 m^2. Room access is done through two entrances, being the main a 1.50 m × 2.10 m double-door and the secondary a 1.00 m × 2.10 m simple-door. A 3.40 m × 0.80 m looking glass reveals internal procedures to the external environment.

A typical operating room layout, consisting of surgical lights, ceiling lights, anesthesia machine, monitor and operating table, is considered for CFD models. These items may influence the air movement and temperature distribution due to buoyancy effect of thermal plumes [36]. Besides, other equipment and furniture also are considered for the baseline model, as shown in Fig. 2. Table 1 reveals further detail on equipment and furniture of the baseline room.

2.1 Scenarios analyzed

In order to validate the CFD model, it was performed a comparison between the numerical solutions and field measurements, which corresponds to **Case 0**. In this scenario, the ventilation system used in operating room is conventional high supply and low exhausts where air is supplied at high level and exhausted at low level. The supply and extract, both of 0.90 m × 0.30 m, are located on the same wall. Although the outlet device is available, in this surgical room, it operates inadequately as air inlet due malfunction. As air escape was observed in the gaps in the main door, they perform as an outlet, being considered as so. Figure 3 displays the geometric modeling of this case. Inlets are represented in green, whereas outlets are highlighted in red. This color scheme is adopted throughout this paper.

Subsequently, four alternative scenarios were simulated, so as to evaluate the effect of different inlet systems and distinct allocation of the outlet device. Apart from Case 0, whose purpose is to fully represent real conditions to validate the CFD model, in the alternative scenarios, the extract operates as outlet, as should be as expected, and gaps were ultimately neglected for its inadequacy to hospital environment.

Regarding the inlet system, type "*a*" cases adopt the actual conventional high supply, whereas type "*b*" ones adopt 4 four-way suppliers of 0.40 m × 0.40 m each. In terms

Table 1 Equipment and furniture characteristics

Item	Quantity	Dimensions (m)	Material
Anesthesia machine	1	0.40 × 0.65 × 1.30	Plastic
Drawer cabinet	1	0.45 × 0.75 × 0.77	Wood
Swivel	1	ϕ 0.31 × 0.65	Stainless steel
Chair	1	0.54 × 0.51 × 0.85	Plastic
Trash can	3	ϕ 0.37 × 0.44	Plastic
Step stool	1	0.16 × 0.40 × 0.32	Stainless steel
Surgical light	1	–	Metal
Electrosurgical generator	1	0.35 × 0.44 × 0.12	Plastic
Hamper	1	ϕ 0.55 × 0.80	Stainless Steel
Instrument table	3	0.50 × 0.40 × 0.80	Stainless steel
Instrument table	2	1.10 × 0.45 × 0.80	Stainless steel
Operating table	1	0.50 × 1.90 × 0.80	Stainless steel
Mayo stand	2	0.32 × 0.48 × 0.85	Stainless steel
IV pole (pedestal)	2	ϕ 0.02 × 1.80	Stainless steel
Pipe medical gases	1	0.17 × 0.23 × 1.40	Metal

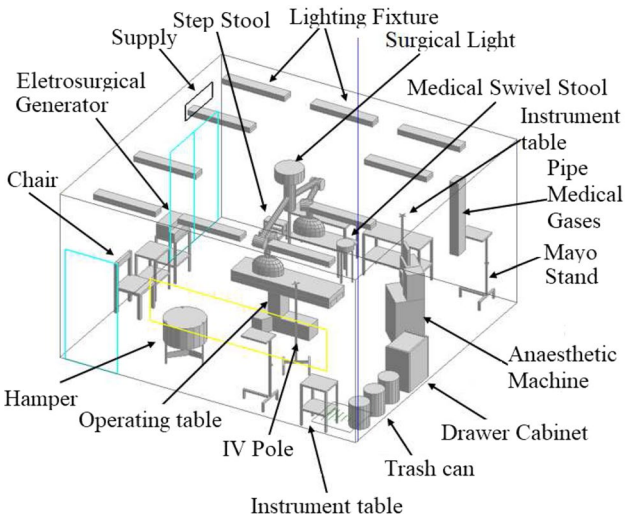

Fig. 2 General view of the baseline model

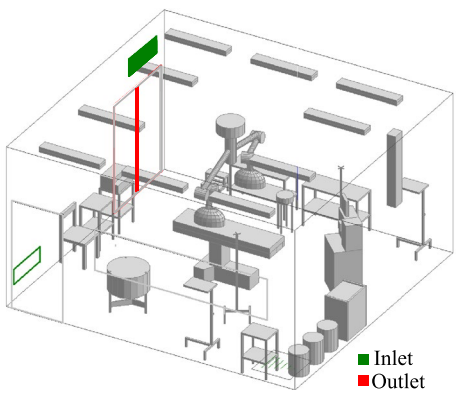

Fig. 3 Geometric model of the Case 0

of exhaust, an outlet of 0.90 m × 0.40m convey the discharge velocity desired. Type "1" cases have their exhaust positioned in the same wall as the real scenario, while type "2" ones have it located on the opposite walls. The outlet device was allocated in two different and unobstructed walls, away from entrances, in order to prevent unbalanced conditions caused by opening and closing. Figure 4 provides four scenarios studied.

3 Mathematical setting and computational approach

In particular to civil construction, CFD approach is exploited to study effects of climate, internal heat gains and HVAC systems (Design Builder [11]), being based on the laws governing three-dimensional flows. The CFD approach was preferable as the aim of this research is not to provide a biological analysis, but a physical investigation on velocity vectors and their potential to carry contaminants.

The conventional CFD software's can be very time-consuming, usually involving laborious modeling. In that sense, the commercial CFD code Design Builder® arises as a powerful tool, as it preprocess complex modeling and automatically suggests mesh geometries and boundary conditions. Through its easiness to reproduce complexity, Design Builder® has the advantages of conceiving a 1:1 model and taking into account all items of furniture, enhancing model's reliability.

Design Builder® recurs to Eulerian approach, in which air is treated as continuum movement as expressed by the equations of conservation of mass, momentum and energy. Assuming airflow's are generally turbulent, the choice for a turbulence model is a necessary. Design Builder® adopts the standard $\kappa - \varepsilon$ turbulence model [23, 40, 41], in which the transport equations of turbulence kinetic energy κ and its dissipation rate ε are involved in the computations.

The $\kappa - \varepsilon$ model is extensively used due to its satisfactory results regarding mechanically ventilated environments [4, 25, 38, 42]. In addition, Pustelnik [31] presents its low-power consumption, in terms of computational processing time and cost, compared to other turbulence models, while preserving relative accuracy.

The generalized form of conservation equation is represented by:

$$\frac{\partial(\rho\phi)}{\partial t} + \frac{\partial}{\partial x_j}(\rho\phi u_j) = \frac{\partial}{\partial x_j}\left(\Gamma_\phi \frac{\partial\phi}{\partial x_j}\right) + S_\phi, \tag{1}$$

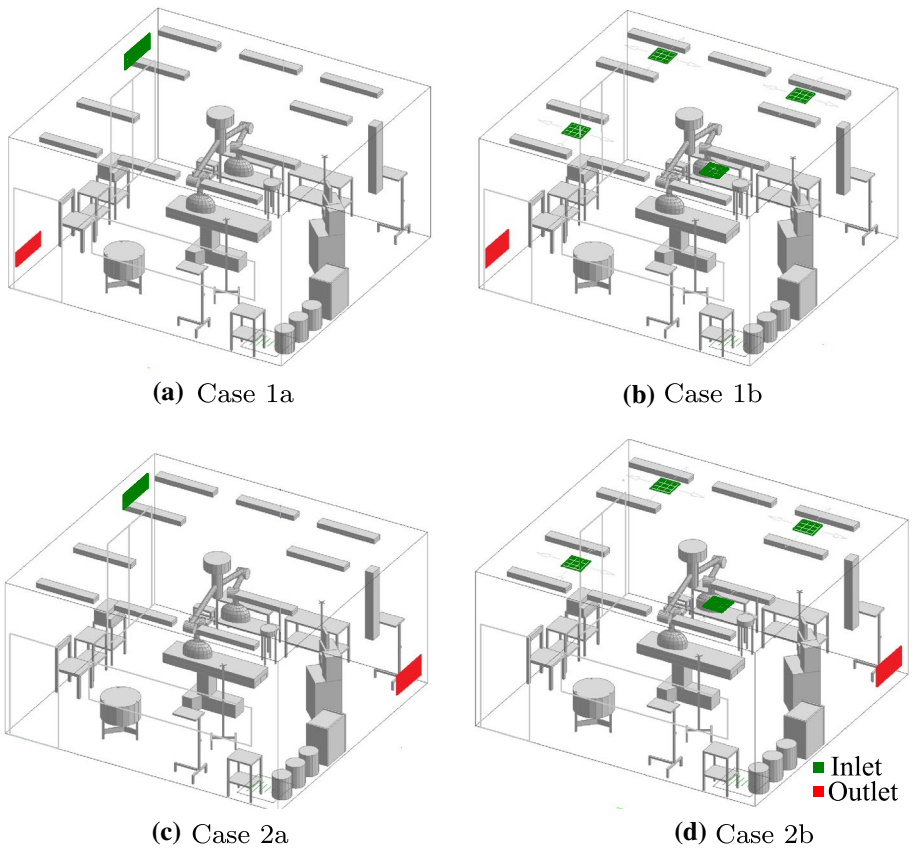

(a) Case 1a **(b)** Case 1b **(c)** Case 2a **(d)** Case 2b

Fig. 4 Alternative scenarios of operating room analyzed

Table 2 Source terms in the transport equations for turbulent flows

Equation	ϕ	Γ_ϕ	S_ϕ
Continuity	1	0	0
Momentum	u_i	μ	$-\frac{\partial p_e}{\partial x_i}+\frac{\partial}{\partial x_j}\left[\nu_t\left(\frac{\partial u_i}{\partial x_j}+\frac{\partial u_j}{\partial x_i}\right)\right]+\rho F$
Energy	T	α	0
Dissipation rate	κ	$\mu+\frac{\nu_t}{\sigma_\kappa}$	$P_\kappa-\varepsilon$
Kinetic energy	ε	$\mu+\frac{\nu_t}{\sigma_\varepsilon}$	$C_{1\varepsilon}\frac{\varepsilon}{\kappa}P_\kappa-C_{2\varepsilon}\frac{\varepsilon^2}{\kappa}$

where ϕ is the dependent variables, ρ is the density, Γ_ϕ is the diffusion coefficient, S_ϕ is a source term and u_j represents the mean velocity components in the x_j directions ($j = 1, 2, 3$).

Airflow is also assumed incompressible, homogeneous and three-dimensional. Table 2 indicates the expressions for the source terms, in which $p_e = p + \frac{2}{3}\frac{1}{\mathrm{Re}}\kappa$ is the effective pressure, μ is the dynamic viscosity and α is coefficient of thermal diffusivity.

The term F, in Table 2, represents the external forces, which in normal wise direction, can be given by Eq. (2):

$$F = \beta(T - T_{\mathrm{ref}}) \times g, \tag{2}$$

where β is the coefficient of thermal expansion, T is temperature, T_{ref} is reference temperature and g is the usual gravitational acceleration field. Furthermore, ν_t represents the eddy viscosity and P_κ the turbulent shear stress production which are, respectively, given by:

$$\nu_t = \rho C_\mu \frac{\kappa^2}{\varepsilon}, \tag{3}$$

$$P_\kappa = \nu_t\left(\frac{\partial u_i}{\partial x_j}+\frac{\partial u_j}{\partial x_i}\right)\frac{\partial u_j}{\partial x_j}. \tag{4}$$

Constants were experimentally obtained [20], assuming the value of: $C_\mu = 0.09$, $C_{1\varepsilon} = 1.44$, $C_{2\varepsilon} = 1.92$, $\sigma_\mu = 1.00$ and $\sigma_\varepsilon = 1.30$.

3.1 Boundary conditions

In order to solve the system of partial differential equations (1), boundary conditions must be clearly defined. In this work, three types boundary conditions were considered: inlet, outlet and rigid-wall boundaries. At the inlet section (fluid entrance), discharge velocity and supply air temperature are specified by the designer, whereas κ and ε are estimated through Eqs. (5) and (6), respectively (more details can be found in Kurokawa et al. [22]):

$$\kappa_{\mathrm{in}} = \frac{3}{2}U_{\mathrm{in}} \times I, \tag{5}$$

$$\varepsilon_{\mathrm{in}} = \frac{C_\mu^{\frac{3}{4}} \times \kappa_{\mathrm{in}}^{\frac{3}{2}}}{l_0}, \tag{6}$$

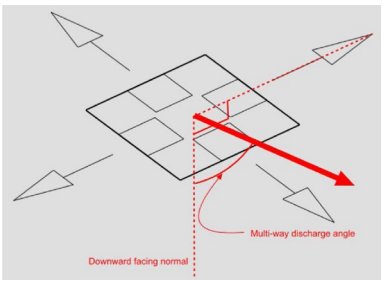

Fig. 6 Discharge angle in ceiling inlets of type 4 four-way supply. *Source* Design Builder®

Fig. 5 Discharge angle in sidewall inlets. *Source* Design Builder®

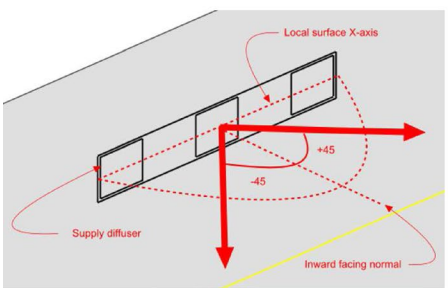

(a) X-axis.

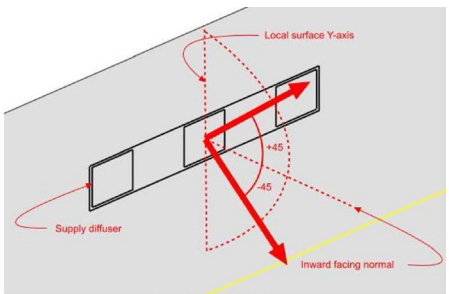

(b) Y-axis.

where I is the turbulence intensity ($I = 8.0 \times 10^{-2}$), l_0 is the turbulent length scale of supply opening and U_{in} the mean inlet flow velocity.

Discharge angles vary according to the type of air supply. Figure 5 presents the discharge angles in sidewall inlets: They are set according to the local surface X and Y-axis (and vice-versa), as well as the adjustable inward facing normal the surface. In this case, inlet airflow is considered unidirectional and uniform. For its part, Fig. 6 presents the discharge angle in ceiling inlets, in which a multiway discharge angle is set from a downward facing normal.

At outlet section (exhaust grilles), the extract flow rate is imposed. It is assumed that the *no-slip* condition is applied on the rigid walls and all mass flux across any solid wall is zero. Besides, heat flux is null, as no exchange of heat transfer was considered (adiabatic). Heat and mass flux were disregarded to room objects, with the exception of lighting fixture, surgical light and anesthesia machine, with constant and uniformly distributed heat flux rate. Moreover, to avoid using too many grid points in the viscous sub-layer, the wall function is used near the walls for variables κ and ε [13, 22, 32, 37].

Design Builder® solves the set of partial differential equations in Eq. (1) by staggered grid finite volume method [27]. Although equations are in transient form, calculations consider a steady state, due to the relevance of the relaxation method in transient terms' behavior, hindering fluctuations in dependent variables and delivering stabler solutions.

The code also resorts to false time step to the pseudo-transient term. The SIMPLE (Semi Implicit Linked Equations) algorithm is adopted to pressure velocity coupling [27]. Finally, diffusion terms and pressure gradients are discretized by central difference scheme, while an upwind scheme is applied to advection terms (for details of these schemes, see [14, 15]).

4 Field measurements and numerical conditions

In order to obtain the indoor environmental parameters such as temperature and velocity of operating room investigated, field measurements were carried out at specified sampling locations during unoccupied period. Measurements were realized in two stages. The first stage revolved around the characterization of the boundary conditions for the simulation, encompassing surfaces, air devices and medical equipments in the surgical room. The second stage had the purpose to obtain velocities and temperatures in control points for the modeling validation.

Three instruments were used to measure and collect the data desired. Apparatus' specifications are summarized in Table 3. Measurements were conduced in stable environment conditions, with the room unoccupied. The measurements were performed in several sessions of 20 minutes.

In the first stage, surface's temperatures were obtained through an infrared thermometer. For its part, an anemometer was used to determine air velocity in various points across the supply and the extract.

Numerical values summarized in averages and standard deviations for surface temperature boundary conditions were obtained for a collection of "n" measurement points. Heat source power boundary conditions were adopted as informed by the items respective manufacturers. Both of these data are presented in Table 4.

On account of being an operating room, doors and windows are expected to be sealed. Nevertheless, the looking glass only was considered as so, as the main door presented a considerable amount of air leakage, which affects air distribution in

Table 4 Boundary condition data from surfaces and items obtained from field measurements and from manufacturer's information

Surface	Heat source (W)	Temperature (°C)
Roof	–	19.0 ± 0.3 ($n = 7$)
Floor	–	18.4 ± 0.9 ($n = 12$)
Wall 1	–	19.8 ± 0.4 ($n = 13$)
Wall 2	–	19.3 ± 0.4 ($n = 12$)
Wall 3	–	20.6 ± 0.6 ($n = 13$)
Wall 4	–	20.0 ± 0.1 ($n = 6$)
Looking glass	–	16.3 ± 0.2 ($n = 3$)
Air supply	–	16.2 ± 0.3 ($n = 2$)
Lighting fixture	64	26.0 ± 1.0 ($n = 5$)
Surgical light	150	52.6 ± 3.1 ($n = 4$)
Anesthesia machine	100	25.0 ± 3.7 ($n = 4$)

Table 3 Measurement instruments and respective measurements

Instrument	#	Function	Operative range	Accuracy
Confortmeter SENSU®	5	Dry bulb temperature	0–60°C	0.2°C
		Relative humidity	5–96%	3%
		Air speed	0–3 m/s	0.04+3%
		Globe temperature	–	0.2°C
Infrared thermometer Extech—MO295	1	Superficial temperature	–	–
Electronic anemometer with rotational system Airflow—LCA-6000-VT	1	Speed	0.25–30 m/s	0.01
		Flow rate	–	–

the room. Experimental data deviations (Table 4) are well within the expected and in accordance with the accuracy of the employed instruments. Larger standard deviations were observed in the surgical lighting system and in the anesthesia machine surface temperature measurements. This is due to the large temperature gradients between adjacent surfaces these types of equipment show. Nonetheless, observed variations do not constitute an impeditive to the ongoing analysis.

Taking into account the observations from Sect. 2.1, numerical values for the inlet and outlet boundary conditions are:

- *Case 0* inflow rates of 375 L/s and 1.67 m/s in the inlet, and 30 L/s in the outlet. Door gaps present an outflow rate of 405 L/s;
- *Alternative cases* equilibrated 400 L/s flow rates and a velocity of 2.5 m/s are observed as no air leakage is considered. The latter in accordance with the noise level lower limit for surgical rooms presented in Brazilian standard NBR 10152 [1]. To wit, outlets require low speed operation, in order to ensure low-pressure drops and facilitate air return, promoting greater efficiency.

In addition, for Cases 0, 1a and 2a (sidewall inlets), discharge angles obtained were −34° and −12° for directions X and Y, respectively. In Cases 1b and 2b (ceiling inlet), discharge angle is 57.3°.

Regarding the second stage of measurements, temperatures and air velocities were measured in control points of the room. For this, confortmeters were strategically positioned in five different points from C_1 to C_5 (see Fig. 7), at a high of 1.10 m, which represents the comfort zone midpoint for people standing as indicated by the standard ISO 7730:2005. Table 5 contains the data obtained (average, standard deviation and number of measured points) from each monitoring point.

Observed deviations for temperature and velocity are within the expected and in accordance with the accuracy of the employed instruments, with the exception of the velocity measured at point C_1. This may be due this is the central point in the room and it is greatly subject to the influence of nearby objects. In such situations, velocity fluctuations are to be expected.

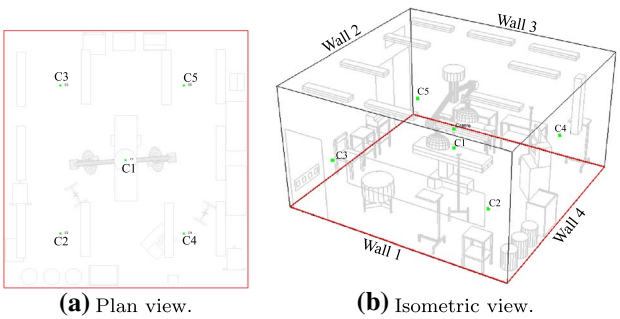

(a) Plan view. **(b)** Isometric view.

Fig. 7 Allocation of the set of confortmeters within non-occupied surgical room

4.1 Geometric modeling

For the geometric modeling, five monitoring cells were placed in the model, in the same exact position as the real scenario (see Fig. 7), in order to compare experimental and computational data.

In terms of mesh, non-uniform grids generated by Design Builder® were adopted, with slight manual changes. These were preferable as the furniture modeled pose a great challenge for the manual definition of grids, as a set of surfaces and vertexes requirements should be met to achieve convergence. Although each cell is properly described by the axes XYZ that contains the surgical room, both of its size and volume depend on the presence of pieces of furniture around or within it.

A coarse grid was primarily adopted. In order to approach the experimental results, two more refined resolutions were preferable. Table 6 presents the specificity of the resolutions used in this study.

The upper limit established for residual absolute values was set to 10^{-5} applicable to: continuity, velocities, energy, κ and ε.

Case 0 was evaluated through the analysis of velocity magnitudes, once the confortmeter from field measurements do not provide details on X, Y, Z components. However, the comparison of alternative scenarios was carried out through a complete vector analysis, in which both magnitude and direction are examined, with the assistance of the angle formed by a vector $\mathbf{v}$ and a plan π whose normal vector is $\mathbf{n}$:

$$\sin\theta = \frac{|\mathbf{v}\cdot\mathbf{n}|}{|\mathbf{v}|\cdot|\mathbf{n}|}. \tag{7}$$

Table 5 Field measurements in monitoring cells

Point	Velocity (m/s)	Temperature (°C)	Measured points
C_1	0.100 ± 0.01	17.59 ± 0.4	$(n = 57)$
C_2	0.320 ± 0.01	18.76 ± 0.2	$(n = 57)$
C_3	0.030 ± 0.01	18.57 ± 0.2	$(n = 57)$
C_4	0.047 ± 0.01	19.06 ± 0.2	$(n = 57)$
C_5	0.067 ± 0.01	19.48 ± 0.2	$(n = 57)$

Table 6 Computational cells adopted

Grid	Cells ($x \times y \times z$)
M1—coarse	$52 \times 48 \times 30$
M2—intermediate	$84 \times 73 \times 39$
M3—fine	$129 \times 105 \times 55$

5 Numerical results

With the aim to validate the model, numerical values for velocities and temperatures from Case 0 are presented in Table 7. Results show that the standard deviation is lower with a higher refinement, indicating that the degree of detail of the grid contributes to reduce modeling's error. In addition, temperatures present greater standard deviations when compared to velocities.

This behavior is also illustrated in Fig. 8. For both velocities and temperatures, M3 points are closer to the line of 45°, which represents the perfect fit of field and model values. This indicates that the higher the refinement, the closer the model values get from the field values.

However, in some control points, deviation was higher in the intermediate mesh M2 than the coarse mesh M1. This is due the fact that meshes are non-uniform, and the relative position of each control point within its cell is different. It is possible that this position was more similar in meshes M1 and M3, allowing for greater relative errors in the intermediate mesh M2.

For its part, Table 8 presents the relative error, which are in general below are below 10%, within tolerance acceptable. Temperatures present a relative error in the range of 1% to 6%, whereas relative errors from velocities are in the region of 4% to 9% if the fine grid is used, validating the model.

C_3 presents a relative error of 20%, which can be explained by the proximity of the cell and the extract, where fluctuations on the discharge velocity in the outlet are found. Although the same behavior is expected in C_5 for its proximity to an inlet device, supply air has a

Table 7 Case 0: velocities and temperatures

Cell	Velocity (m/s)			Temperatures (°C)		
	M1	M2	M3	M1	M2	M3
C_1	0.203	0.055	0.091	18.97	18.80	18.72
C_2	0.288	0.226	0.341	17.86	18.33	18.33
C_3	0.083	0.019	0.024	18.15	18.18	18.47
C_4	0.044	0.059	0.049	18.27	18.51	18.63
C_5	0.065	0.062	0.064	18.06	18.36	18.43
SD	0.069	0.061	0.014	1.36	1.06	0.96

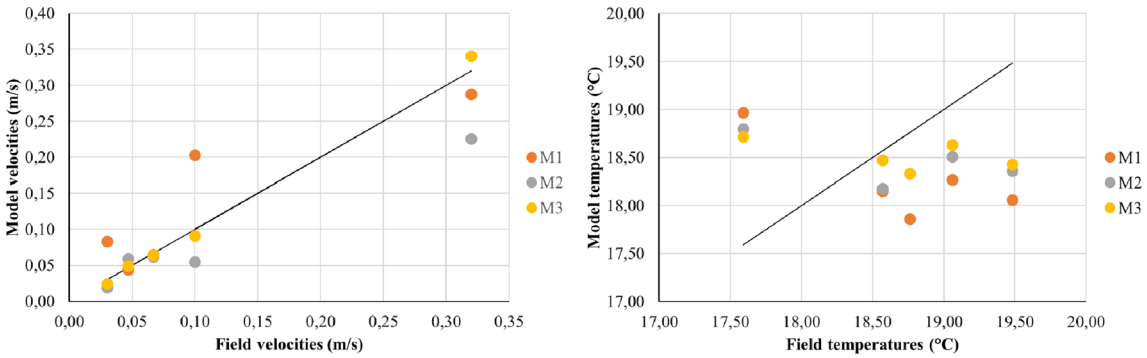

(a) Velocities. **(b)** Temperatures.

Fig. 8 Field values *x* model values

Table 8 Case 0: relative error

Cell	Velocity (m/s)			Temperature (° C)		
	M1	M2	M3	M1	M2	M3
C_1	1.030	0.450	0.090	0.078	0.069	0.064
C_2	0.100	0.290	0.066	0.048	0.023	0.023
C_3	1.760	0.370	0.200	0.023	0.021	0.005
C_4	0.064	0.260	0.043	0.041	0.029	0.023
C_5	0.030	0.074	0.045	0.073	0.057	0.054

Table 9 Velocities in Case 0 and Case 1a

Cell	Velocity (m/s)		Relative ΔV
	Case 0	Case 1a	
C_1	0.091	0.071	0.220
C_2	0.341	0.137	0.598
C_3	0.024	0.078	2.250
C_4	0.049	0.086	0.755
C_5	0.064	0.079	0.234

Table 10 Temperatures in Case 0 and Case 1a

Cell	Temperature (° C)		Relative ΔV
	Case 0	Case 1a	
C_1	18.72	18.51	0.01
C_2	18.33	18.45	0.01
C_3	18.47	18.34	0.01
C_4	18.63	18.29	0.02
C_5	18.43	18.33	0.01

considerably higher flow rate and velocity, resulting in a more stable behavior.

In case no gap in the door is considered, the comparison between Case 0 and Case 1a, velocities in monitoring cells are strongly affected, as indicated in Table 9.

In particular, C_3 cell presents the greatest difference of them all, what can be explained by the fact that the extract was working as an inflow device. Conversely, temperatures face a reduction—with the exception of cell C_2—being the relative difference in the region of 0.01 and 0.02, greater in C_4 cell (Table 10).

Table 11 presents velocities components and their magnitudes from the alternative cases, while Table 12 presents angles between vectors and plans *XY*, *XZ* and *YZ*. Maximum variance is in the region of 1.1×10^{-2} (V_{Y-C1}), and minimum is around 6.9×10^{-7} (V_{Z-C1}).

According to Fig. 9, type *a* cases present lower variance than type *b* ones. This suggests that, if extract position is altered, sidewall inflow is less susceptible to velocity fluctuation than ceiling diffusion. In addition, it indicates that a change in inflow system presents a greater influence to air velocity than a change in extract position.

For its part, Fig. 10 illustrates graphically the angles previously presented in Table 12. It is possible to affirm that, despite the considerable variance, cases with the same inflow system have in general a smaller angle difference when compared to cases with same outlet position, irrespective of plan analyzed. In other words, angles from type a cases are closer to one another, pattern also observed in type *b* ones. This proximity is sharper in type *b* cases.

Table 11 Alternative cases: velocities

Cell	1a	1b	2a	2b	Var
u-velocity component					
C_1	0.019	0.053	− 0.004	0.015	4.2×10^{-4}
C_2	− 0.082	0.129	− 0.050	0.106	8.6×10^{-3}
C_3	− 0.004	− 0.062	0.061	− 0.117	4.4×10^{-3}
C_4	− 0.031	− 0.023	− 0.017	− 0.012	5.0×10^{-5}
C_5	0.071	0.025	0.089	0.049	5.7×10^{-4}
v-velocity component					
C_1	− 0.068	0.167	− 0.041	0.141	1.1×10^{-2}
C_2	0.108	0.067	0.094	− 0.027	2.8×10^{-3}
C_3	0.078	0.002	0.114	− 0.092	6.2×10^{-3}
C_4	0.077	0.106	− 0.061	0.057	4.0×10^{-3}
C_5	− 0.022	0.162	− 0.034	0.052	6.1×10^{-3}
w-velocity component					
C_1	0.001	0.000	0.001	− 0.001	6.9×10^{-7}
C_2	0.017	0.024	0.017	− 0.031	4.8×10^{-4}
C_3	− 0.002	− 0.020	− 0.012	− 0.102	1.6×10^{-3}
C_4	− 0.021	0.090	− 0.061	0.031	3.2×10^{-3}
C_5	0.026	0.060	− 0.014	0.060	9.3×10^{-4}
V					
C_1	0.071	0.175	0.041	0.142	2.9×10^{-3}
C_2	0.137	0.147	0.108	0.114	2.6×10^{-4}
C_3	0.078	0.065	0.130	0.180	2.1×10^{-3}
C_4	0.086	0.141	0.088	0.066	7.7×10^{-4}
C_5	0.079	0.175	0.096	0.093	1.4×10^{-3}

Table 12 Angles (°) between vector and plan

Cell	1a	1b	2a	2b
θ_{XY}				
C_1	− 29.386	62.608	− 50.550	51.071
C_2	7.731	70.169	16.770	29.429
C_3	42.047	− 40.613	72.360	− 54.990
C_4	22.327	24.608	− 38.850	28.831
C_5	26.104	49.247	23.820	49.948
θ_{XZ}				
C_1	11.553	12.351	− 2.951	4.003
C_2	− 19.652	47.25	− 12.500	27.805
C_3	3.113	− 62.826	15.480	− 59.119
C_4	25.432	19.642	38.850	11.748
C_5	60.577	20.141	33.420	55.699
θ_{YZ}				
C_1	− 42.14	42.375	− 43.350	44.278
C_2	40.298	25.897	46.720	− 21.145
C_3	43.460	− 11.261	33.740	− 49.487
C_4	27.547	79.522	− 78.850	70.566
C_5	2.058	64.067	− 20.640	58.084

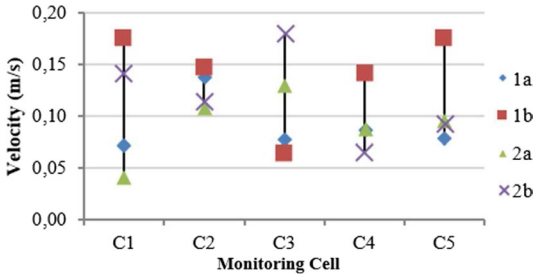

Fig. 9 Velocities and high-low lines

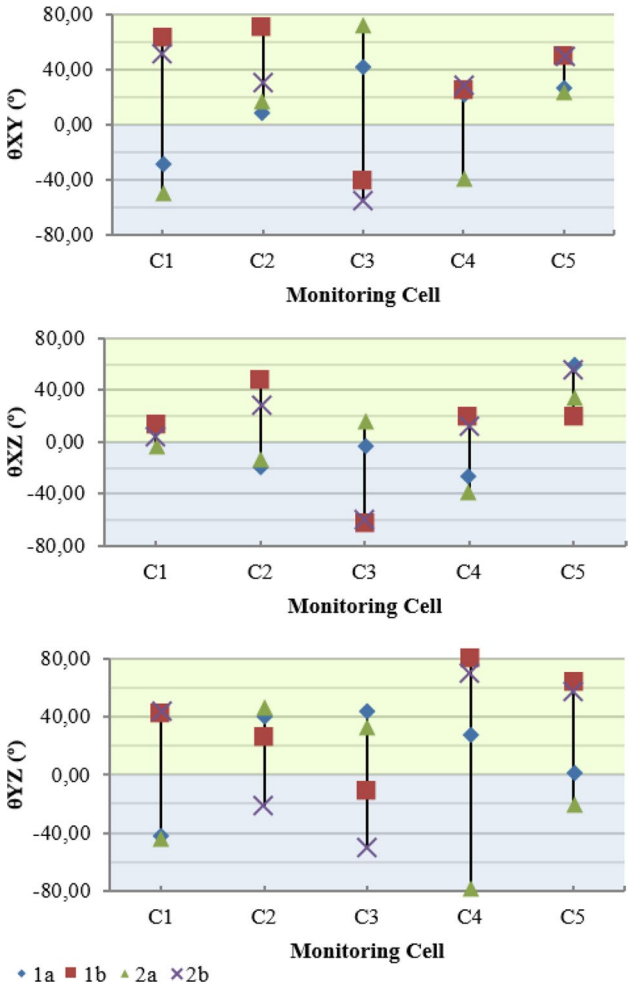

Fig. 10 Angles between vectors and planes

Figures 11 and 12 present the velocity vectors that define air motion in the surgical room, for each scenario and section view. In these pictures, vectors' magnitude is represented by a predefined color scale, being blue associated with lower values, ad red with higher values. Vector's direction indicates from and to the air is dislocated, revealing also whether the air meets any object along the way.

Concerning the *XZ* plan, Fig. 11 reveals that velocity vectors have a tendency to move toward the operating table, in all cases analyzed. However, type *a* cases present vectors with lower magnitude in the center of the room, making it more difficult for it to carry undesirable particles. Conversely, type *b* cases have less air stratification and air vortex than the previous cases.

In terms of *YZ* plan (Fig. 12), type *b* cases still present greater velocity magnitudes, while type *a* cases conserve their low magnitudes pattern. Nonetheless, it is important to highlight that, in both cases with sidewall inlet, an upward motion is observed near the operating table, with air moving from the soiled to the clean zone.

Moreover, although ASHRAE [3] presents ceiling inflows as preferable in hospital environments to prevent air recirculation, this system presented more substantial air vortex than sidewall inlet, especially in room's fringe, with its position depending on extract allocation. As a matter of a fact, its allocation is a paramount factor to be considered when designing operating rooms: while Case 1b has an air recirculation above the operating table, Case 2b illustrates clean air being directly jetted in it.

The analysis of angles, together with the flow vectors, indicates that the use of High Supply promotes a more adequate environment for an operating room, as C_1 presents negative angles and, consequently, vectors generally leaving this surface. This behavior is preferable in a scenario in which particulate material is present and prejudicial for sanitary requirements. Conversely, the four-way suppliers presented a greater velocity magnitude close to the floor, which could entail the lifting of particulate material in this surface.

Table 13 presents the temperatures obtained from alternative cases. Cases type 1 presents a variance of 6.00×10^{-3}, while type 2 cases have a variance of 1.50×10^{-2}. Type *a* and *b* cases present, respectively, a variance of 2.62×10^{-2} and 7.23×10^{-3}. Hence, a small fluctuation is found in type 1 and *b* cases.

6 Concluding remarks

Firstly, it is important to highlight the pertinence of Design Builder® for this research. By taking into account all items of furniture, a 1:1 scale, and more important, the non-uniform grid with an adequate refinement, the standard deviation was 0.014 for velocities and 0.959 for temperatures, whereas the relative error was limited to 9% in 90% of the time. In that sense, the adequate use of this software is strongly recommended for investigations concerning both analysis.

In respect of the study case analyzed, it is possible to affirm that gap control should be worthy of great attention, especially when it comes to hospital environment. By

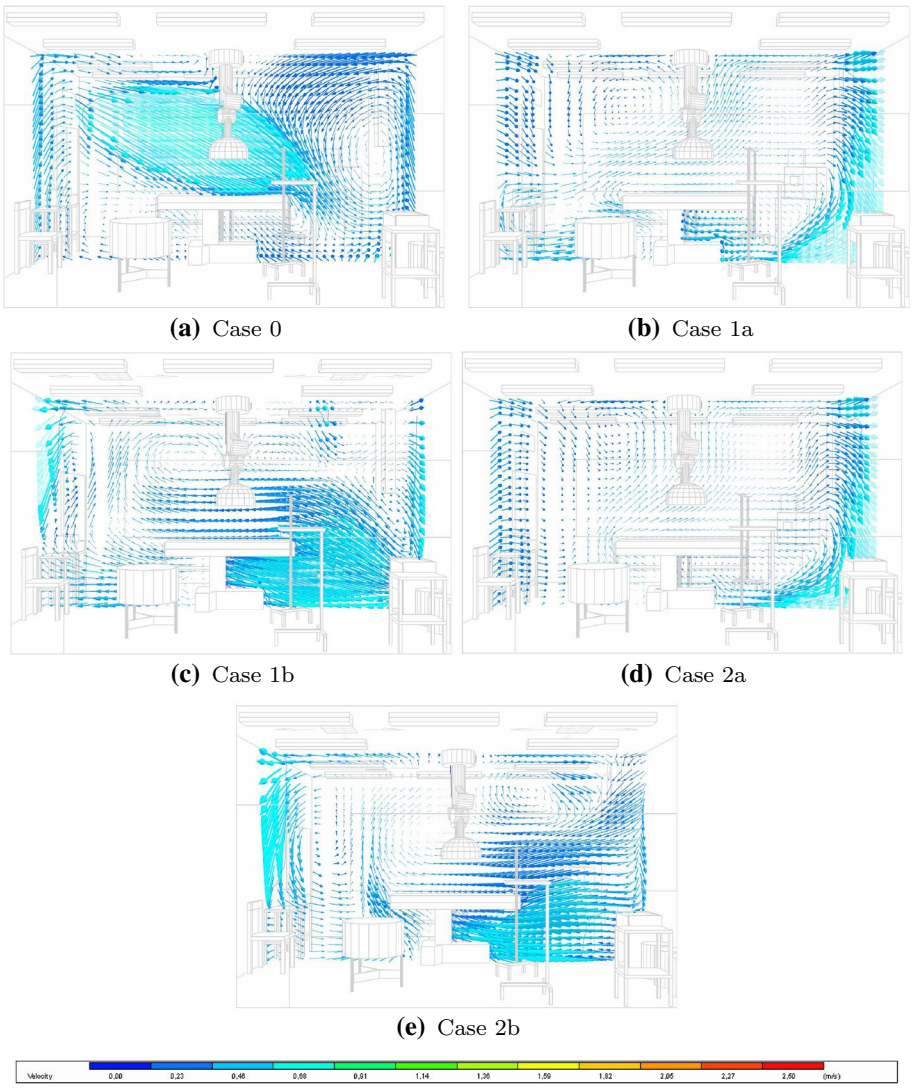

Fig. 11 Flow vectors: plan *XZ*

altering flow conditions, gaps alter pressure conditions, so that outlet ended up performing as an inflow device, which is not in accordance with to sanitary requirements.

In addition, it is possible to infer that velocities are less susceptible of fluctuation if extract position is altered in sidewall inflow system. Also, it indicates that a change in inflow system presents a greater influence to air velocity than a change in extract position.

Regarding air motion, all cases presented are in accordance with ASHRAE [2] optimum diffusion, due to the fact that air scrub the ceiling surface, promoting air renewal. This is due to the discharge conditions: the acuter the angle, the more tendency the fluid has to be directed to peripheral areas. In addition, the higher the magnitude, the greater its horizontal reach. In that sense, the inlet conditions adopted favor inflow air primarily contact with soiled area.

However, neither case analyzed is integrally adequate to flow conditions pursued on a hospital environment. Nonetheless, this research has as scientific contribution the discussion of the usage of computing tool, in terms of modeling furniture and refine meshes, allowing for small errors. Moreover, it presents how the choice for the air inflow system and positioning of outlet devices are instrumental to determine air motion and adequacy regarding the environment.

As a suggestion for a continued research, two aspects could be evaluated: the analysis of the particulate material and the consideration of different discharge angles, as adjustable-angle inlets are largely adopted, especially for field adjustments and adequacy to cool-air-sensitive patients.

Fig. 12 Flow vectors: plan *YZ*

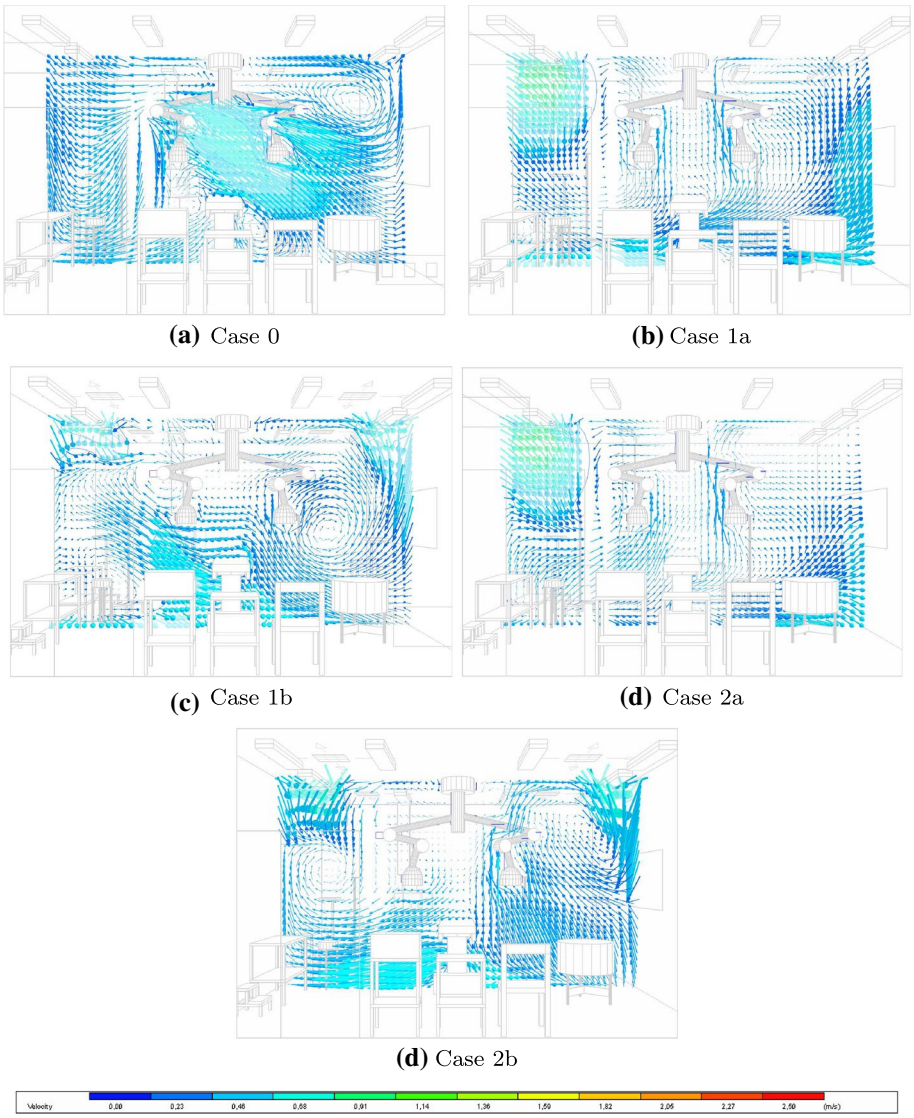

Table 13 Alternative cases: temperatures

Cell	1-a	1-b	2-a	2-b	Var
C_1	18.51	18.40	18.75	18.50	1.7×10^{-2}
C_2	18.45	18.36	18.74	18.42	2.1×10^{-2}
C_3	18.34	18.53	18.54	18.37	8.2×10^{-3}
C_4	18.29	18.48	18.61	18.54	1.4×10^{-2}
C_5	18.33	18.44	18.68	18.65	2.1×10^{-2}

Acknowledgements Support for this research was provided by the Brazilian agency CNPq (Conselho Nacional de Desenvolvimento Científico e Tecnológico) under Grants 311440/2013-4 and 457248/2014-9.

Compliance with ethical standards

Conflict of interest The authors declare that there is no conflict of interest.

References

1. l Associação Brasileira de Normas Técnicas (2005) NBR10152: Níveis de ruído para conforto acústico. Rio de Janeiro, Brazil
2. ASHRAE (2003) ASHRAE handbook: heating, ventilating and air conditioning design manual for hospitals and clinics. American Society of Heating, Refrigerating and Air-Conditioning Engineers, Atlanta
3. ASHRAE (2009) ASHRAE handbook: space air diffusion. Fundamentals. American Society of Heating, Refrigerating and Air-Conditioning Engineers, Atlanta
4. Attia AE-H, Helw ME, Teamah H-AM (2013) Three-dimensional thermal comfort analysis for hospital operating room with the effect of door gradually opened part (I) effect on velocity and temperature distributions. CFD Lett 5(1):6–19
5. Batchelor GK (1967) An introduction of fluid dynamics. Cambridge University Press, Cambridge
6. Beck WC, Frank F (1973) The open door in the operating room. Am J Surg 125:592–595
7. BRASIL (2003) Ministério da Saúde. Agência Nacional de Vigilância Sanitária (ANVISA). Resolução – **RE n. 9, de 16 de janeiro de 2003**. Determina a publicação de Orientação Técnica

elaborada por Grupo Técnico Assessor, sobre Padões Referenciais de Qualidade do Ar Interior, em ambientes climatizados artificialemente de uso público ou coletivo
8. Cheong KWD, Phua SY (2006) Development of ventilation design strategy for effective removal of pollutant in the isolations room of a hospital. Build Environ 4:1161–1170
9. Chow T, Yang X (2003) Performance of ventilation system in a no-standard operation room. Division of Building Science and Technology, City University of Hong Kong, Hong Kong
10. Da Silva CA (2016) Airflow analysis in an operating room for simulation CFD (in Portuguese). M.Sc. dissertation, University of Sao Paulo, Brazil
11. Design Builder n.d. Design Builder CFD. http://www.designbuildersoftware.com/docs/DesignBuilder_CFD_DraftManual.pdf. Accessed 24 Oct 2017
12. Felix VB (2008) Thermal comfort and local discomfort conditions in surgical rooms (in Portuguese). M.Sc. dissertation, University of Sao Paulo, Brazil
13. Ferreira VG, Brandi AC, Kurokawa FA, Seleghim P Jr, Castello AF, Cuminato JA (2007) Incompressible turbulent flow simulation using the $\kappa $-$\varepsilon $ model and upwind schemes. Math Probl Eng, Article ID 12741, pp 1–26
14. Ferreira VG, Kurokawa FA, Queiroz RAB, Kaibara MK, Oishi CM, Cuminato JA, Castello AF, Tomé MF, McKee S (2009) Assessment of a high-order finite difference upwind scheme for the simulation of convection–diffusion problems. Int J Numer Methods Fluids 60:1–26
15. Ferreira VG, Kurokawa FA, Oishi CM, Kaibara MK, Castello AF, Cuminato JA (2009) Evaluation of a bounded high order upwind scheme for 3D incompressible free surface flow computations. Math Comput Simul 23:419–445
16. Fox R, McDonald AT (1995) Introdução à Mecânica dos Fluídos. Livros Técnicos e Científicos—LCT
17. Gosdena PE, Macgowana AP, Bannister GC (1998) Importance of air quality and related factors in the prevention of infection in orthopedic implant surgery. J Hosp Infect 39:173–180
18. Hathway EA, Noakes CJ, Sleigh PA, Fletcher LA (2011) CFD simulation of airborne pathogen transport due to human activities. Build Environ 46:2500–2511
19. Hirsch C (1988) Numerical computation of internal and external flows, vol 1, 2nd edn. Wiley, Chichester
20. Jones W, Launder B (1972) The prediction of laminarization with a two-equation model of turbulence. Int J Heat Mass Transf 15:301–314
21. Khankari K (2016) Patient room HVAC. ASHRAE J 58(6):16–26
22. Kurokawa FA, Corrêa L, Queiroz RAB (2018) Numerical simulation of 3D unsteady turbulent free surface flows using $\kappa - \varepsilon $ model and ADBQUICKEST scheme. J Braz Soc Mech Scl 40:202
23. Launder BE, Spalding DB (1974) The numerical computation of turbulent flows. Comput Method Appl Mech 3:269–289
24. Milner JT, Dimitroulopoulou C, Apsimon HN (2004) Indoor concentrations in buildings from sources outdoors. UK Atmospheric Dispersion Modeling Liaison Committee, ADMLC/2004/2
25. Mousavi ES, Grosskopf KR (2015) Ventilation rates and airflow pathways in patient rooms: a case study of bioaerosol containment and removal. Ann Occup Hyg 59(9):1190–1199
26. Nilsen PV (2004) Computational fluid dynamics and room air movement. Indoor Air Cph 14(7):134–143
27. Patankar SV (1980) Numerical heat transfer and fluid flow. Hemisphere Publishing Corporation, Washington
28. Pereira ML, Tribess A (2005) Sistemas de tratamento de ar em salas cirúrgicas: estudo da distribuição de partículas a avaliação da contaminação aérea. VIII Congresso Ibero-americano de Aire Acondicionado y Refrigeración – CIAR Montevidéo
29. Pereira ML (2008) Measurement, prediction and analysis of airborne particles in surgical rooms (in Portuguese). D.Sc. thesis, University of Sao Paulo, Brazil
30. Posner JD, Buchanan CR, Dunn-Rankin D (2003) Measurement and prediction of indoor air flow in a model room. Energy Build 35(5):515–526
31. Pustelnik M (2005) Avaliação numérica de ambientes com insuflamento de ar frio pelo piso. M.Sc. dissertation, University of Sao Paulo, Brazil
32. Queiroz RAB, Kurokawa FA, Candezano MAC, Corrêa L (2017) Numerical investigations of turbulent free surface flows using TOPUS scheme. Comput Appl Math 36:1145–1160
33. Santana EGF (2013) Thermal comfort and CO_{2} concentration in air conditioned operating rooms and waiting rooms for patients (in Portuguese). M.Sc. dissertation, University of Sao Paulo, Brazil
34. Steverson TC (2008) Experimental investigation of hospital operating room air distribution. Master dissertation, Georgia Institute of Technology, Atlanta
35. Sadrizadeh S, Pantelic J, Shermana M, Clark J, Abouali O (2018) Airborne particle dispersion to an operating room environment during sliding and hinged door opening. J Infect Public Health 11:631–635
36. Sinha SL, Arora RC, Roy S (2002) Numerical simulation of room air distribution with Buoyancy at different outlet locations. Fluid Mech Fluid Power 181–190
37. Sondak DL, Pletcher RH (1995) Application of wall functions to generalized nonorthogonal curvilinear coordinate systems. AIAA J 33:33–41
38. Thool SW, Sinha SL (2014) Numerical simulation and comparison of two conventional ventilation systems of operating room in the view of contamination control. Int J Comput Appl 85(5):31–35
39. Waked R (2011) Effect of ventilation strategies on infection control inside operating theatres. Eng Appl Comput Fluid 4(1):1–16
40. Wilcox DC (1993) Turbulence modeling for CFD. DCW Industries, California
41. Yakhot V, Orszag SA, Tangam S, Gatsky TB, Speziale CG (1992) Development of turbulence models for shear flows by double expansion technique. Phys Fluids 4:1510–1520
42. Zhao B, Li X, Yan QA (2003) A simplified system for indoor airflow simulation. Build Environ 38(4):543–552